

Definition and quantification of acute inflammatory white matter injury in the immature brain by MRI/MRS at high magnetic field

Gregory A. Lodygensky^{1,2,3}, Nicolas Kunz^{1,4}, Elodie Perroud¹, Emmanuel Somme¹, Vladimir Mlynarik⁴, Petra S. Hüppi¹, Rolf Gruetter⁴ and Stéphane V. Sizonenko¹

BACKGROUND: Lipopolysaccharide (LPS) injection in the corpus callosum (CC) of rat pups results in diffuse white matter injury similar to the main neuropathology of preterm infants. The aim of this study was to characterize the structural and metabolic markers of acute inflammatory injury by high-field magnetic resonance imaging (MRI) magnetic resonance spectroscopy (MRS) *in vivo*.

METHODS: Twenty-four hours after a 1-mg/kg injection of LPS in postnatal day 3 rat pups, diffusion tensor imaging and proton nuclear magnetic spectroscopy (¹H NMR) were analyzed in conjunction to determine markers of cell death and inflammation using immunohistochemistry and gene expression.

RESULTS: MRI and MRS in the CC revealed an increase in lactate and free lipids and a decrease of the apparent diffusion coefficient. Detailed evaluation of the CC showed a marked apoptotic response assessed by fractin expression. Interestingly, the degree of reduction in the apparent diffusion coefficient correlated strongly with the natural logarithm of fractin expression, in the same region of interest. LPS injection further resulted in increased activated microglia clustered in the cingulum, widespread astrogliosis, and increased expression of genes for interleukin (IL)-1, IL-6, and tumor necrosis factor.

CONCLUSION: This model was able to reproduce the typical MRI hallmarks of acute diffuse white matter injury seen in preterm infants and allowed the evaluation of *in vivo* biomarkers of acute neuropathology after inflammatory challenge.

White matter injury in the preterm infant can lead to the most severe manifestation, namely cystic periventricular leukomalacia (PVL), with significant clinical impairment such as spastic diplegia (1), cognitive visual dysfunction (2), delayed visual maturation, strabismus, visual field defects, and attention deficit (3). Cystic PVL can be readily identified by ultrasonography, but in case of milder and more diffuse injury, the reliability of this technique comes into question (4). When investigated by T2 hyperintensities in magnetic resonance

imaging (MRI), diffuse white matter injury without cysts was seen in up to 79% of preterm infants imaged at term (5), later shown to be associated with an increased T2 relaxation time constant (6) and shown to correlate with impaired neurodevelopmental outcome if moderate or severe (7). PVL has been associated with coagulation necrosis in the white matter adjacent to the external angle of ventricles, preoligodendrocyte death, microglial activation, and astrogliosis (8). Recently, apoptosis in the white matter as well as basal ganglia injury and associated cortical injury have been characterized in the preterm brain (9–11).

Hypoxic–ischemic and inflammatory injuries are the two main physiopathological mechanisms involved in PVL (12). Several animal models have been developed replicating these mechanisms either separately (i) using the Rice–Vannucci model on very immature animals (13), (ii) by exposing the fetus to intrauterine infection (14), or (iii) by lipopolysaccharide (LPS) administration alone (15) or in combination with a hypoxic–ischemic insult, showing the potentiating effect of LPS (16). Detailed *ex vivo* intermediate and long-term changes have been studied with MRI 10 d following inflammation in premyelinating fetal sheep (15,17) and 1 mo following inflammation in a neonatal mouse model (18). Fetal sheep exposed to LPS were shown to suffer a pattern of injury with striking similarities to preterm infants when scanned at term, with periventricular cysts, gliotic scars, increased white matter T2 intensity, and thinning of the corpus callosum with increased radial diffusivity (15,17). Using *ex vivo* MRI, newborn mice exposed to interleukin (IL)-1 β showed a similar increase in radial diffusivity in the white matter corresponding to axonal thinning and altered myelination (18) when assessed 30 d postinjury. Similarly, rats exposed to LPS at 3 d of life were shown to have an increased radial diffusivity at 21 d of life using *ex vivo* high-field MRI (19).

To establish correlations between known histopathological changes found in PVL and acute *in vivo* changes in MRI, we chose an inflammatory model found to be highly reproducible

¹Department of Pediatrics, Division of Child Development & Growth, University of Geneva, Geneva, Switzerland; ²Department of Pediatrics, Neonatal ICU, Research Center, CHU Sainte-Justine, Montréal, Québec, Canada; ³Montreal Heart Institute, Research Center, University of Montreal, Montréal, Québec, Canada; ⁴Laboratory for Functional and Metabolic Imaging, École Polytechnique Fédérale de Lausanne, Lausanne, Switzerland. Correspondence: Gregory A. Lodygensky (ga.lodygensky@umontreal.ca)

Received 2 May 2013; accepted 7 September 2013; advance online publication 29 January 2014. doi:10.1038/pr.2013.242

and relevant to the injury seen in the preterm brain using an injection of LPS in the corpus callosum (20). This model has been initially developed on postnatal day 5 (P5) rat pups that have a maturational equivalence of 28–32 wk' gestation in humans (21). One initial study on conventional MRI and diffusion tensor imaging (DTI) has shown distinct brain alterations after LPS exposure in P5 rat pups, with symmetrical ventricular dilatation, increased T2 relaxation time constant, and an initial reduction of the apparent diffusion coefficient (ADC), followed, after a few days, by an increased ADC value together with an increase in radial diffusivity (21). In addition to what is seen in PVL, this model has separately been shown to induce a strong astrogliosis, white matter necrosis, apoptosis; increased microglial activation with increased IL-1 β , IL-6, and tumor necrosis factor (TNF)- α ; evidence of lipid peroxidation; as well as neurobehavioral deficits such as dysfunction in the beam-walking test and learning and memory deficits (20,22,23). To define the brain tissue alterations in the very immature brain, similar to the more diffuse white matter injury seen in the preterm infant born before 28 wk, the aim of the current study was to noninvasively characterize the acute inflammatory injury in the very immature P3 rat brain corresponding to 24–28 wk of human gestation by MRI, DTI, and magnetic resonance spectroscopy (MRS) (13,24). Noninvasive markers would allow the detection and quantification of ongoing inflammatory injury during the immediate neonatal period in these extremely immature rat pups.

RESULTS

Spectroscopy

Twenty-four hours after LPS injection into the corpus callosum of rat pups, 13 metabolites were identified locally (**Figure 1**). Among these metabolites, acute LPS exposure caused an increase in lactate and macromolecules. Lactate quantification by the LCModel (Stephen Provencher INC, Oakville, Ontario, Canada) showed a significant increase in LPS-exposed pups when compared with pups injected with normal saline (NaCl) alone (Lac-LPS: 3.18 ± 0.388 $\mu\text{mol/g}$, Lac-NaCl: 1.96 ± 0.212 $\mu\text{mol/g}$; $P = 0.01$). When analyzed separately, only males had a significant lactate increase ((Lac-LPS: 3.74 ± 0.518 $\mu\text{mol/g}$, Lac-NaCl: 1.85 ± 0.255 $\mu\text{mol/g}$; $P = 0.01$). There was no correlation between lactate concentration and the quantification of apoptosis by fractin expression in the corpus callosum. There was an 11% increase in macromolecules (Mac) in LPS-exposed brains, which trended toward significance (Mac-LPS: 1.67 ± 0.046 $\mu\text{mol/g}$, Mac-NaCl: 1.5 ± 0.085 $\mu\text{mol/g}$; $P = 0.08$). Interestingly, in animals exposed to LPS, we identified free lipids, with a measurable concentration of 12.34 ± 1.6 $\mu\text{mol/g}$ (**Figure 1**). There was no significant correlation between the lipid signal and fractin expression, with the caveat that NaCl animals were not included, because they did not show a lipid peak. Other quantified metabolites were not different between the two groups.

DTI Study

ADC maps, known to be highly sensitive to physiological imbalance, revealed a visually recognizable and significant

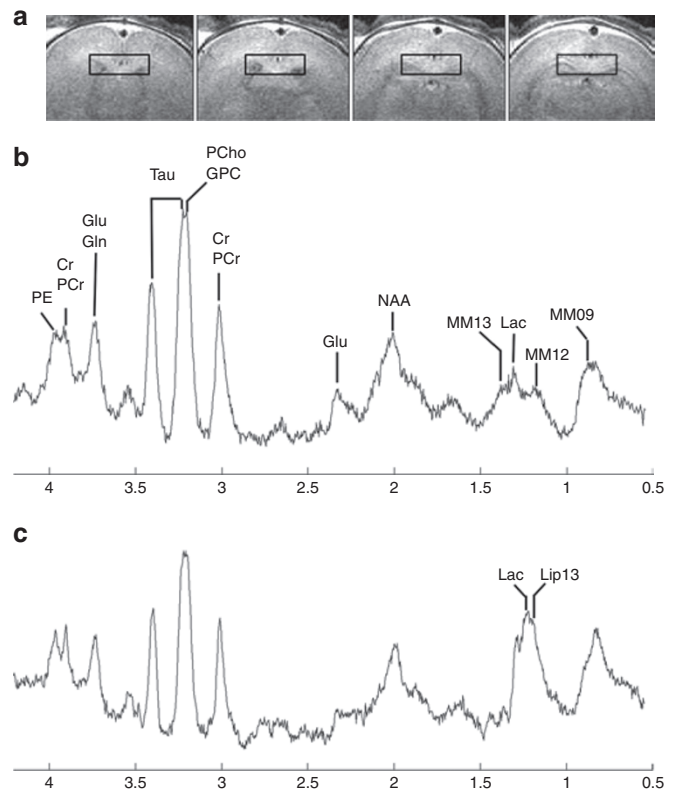


Figure 1. *In vivo* proton nuclear magnetic resonance spectroscopy: (a) spectrum acquired in a volume of 7.5 μl covering the corpus callosum (highlighted in black on the T2-weighted inset fast spin echo coronal images on P4 rat pups 24 h after (b) 0.9% NaCl or (c) lipopolysaccharide (LPS) injection. Thirteen metabolites were identified. Note the increase in lactate and the appearance of the lipid peak at 1.3 ppm, Lip13, in the LPS group. Cr, creatine; Gln, glutamine; Glu, glutamate; GPC, glycerophosphorylcholine; Lac, lactate; Lip13, lipid peak at 1.3 ppm of a methylene carbon backbone; MM12, macromolecule peak; MM13, macromolecule peak; NAA, *N*-acetylaspartate; PCr, phosphocreatine; PE, phosphorylethanolamine; Tau, taurine.

reduction of the ADC value in the corpus callosum (LPS: 1.04 ± 0.02 , NaCl: 1.23 ± 0.01 $\mu\text{m}^2/\text{ms}$; $P = 0.0001$; **Figure 2**). In the same region of interest, the radial (LPS: 0.64 ± 0.01 , NaCl: 0.83 ± 0.01 $\mu\text{m}^2/\text{ms}$; $P < 0.0001$) and axial (LPS: 1.82 ± 0.04 , NaCl: 2.01 ± 0.02 $\mu\text{m}^2/\text{ms}$; $P = 0.0002$) diffusivity values were also reduced (**Figure 2**). Because of a mild increase of fractin expression in the striatum (see below), we quantified ADC in the corresponding area, which revealed a significant reduction of ADC in the LPS-exposed animals (LPS: 0.97 ± 0.01 , NaCl: 1 ± 0.015 $\mu\text{m}^2/\text{ms}$; $P = 0.03$) and a significant reduction of radial diffusivity (LPS: 0.85 ± 0.01 , NaCl: 0.89 ± 0.01 $\mu\text{m}^2/\text{ms}$; $P = 0.02$; **Figure 2c**). An additional region of interest just below the corpus callosum at the level of the head of the hippocampus was analyzed to exclude a systematic bias and it showed no difference between groups in terms of ADC (LPS: 1.04 ± 0.02 $\mu\text{m}^2/\text{ms}$; NaCl: 1.06 ± 0.03 $\mu\text{m}^2/\text{ms}$).

Histology

Microglial activation. LPS exposure was followed by an intense microglial reaction (**Figure 3a,b**), with densely packed

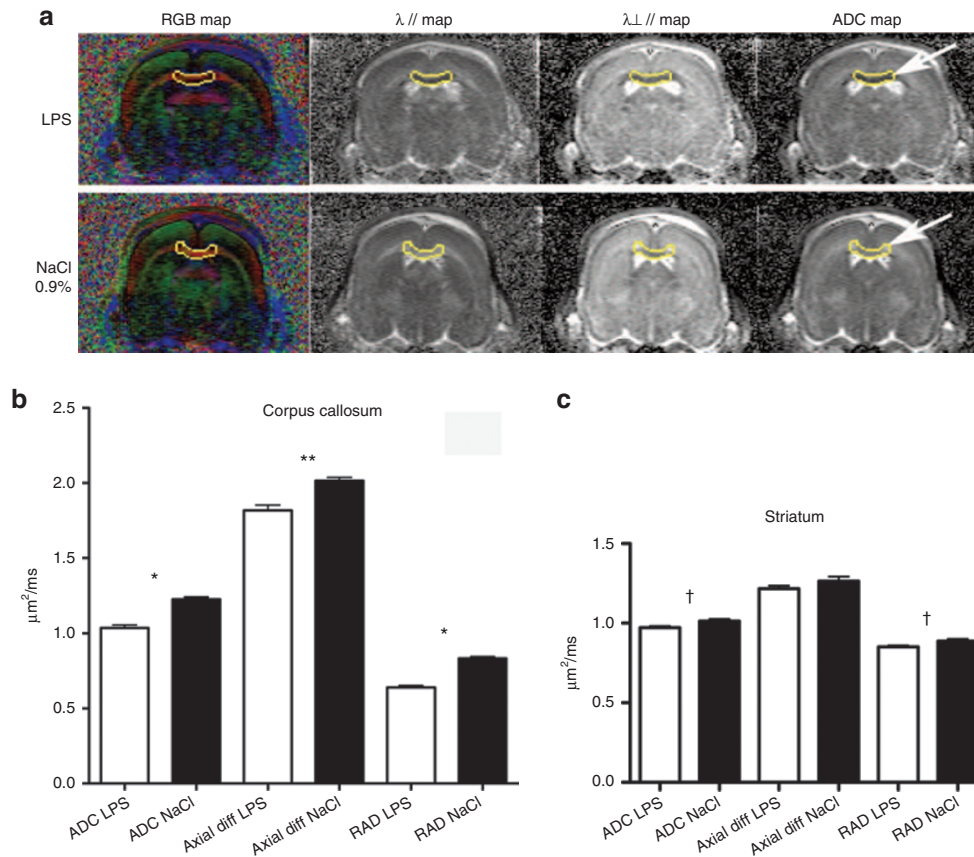


Figure 2. *In vivo* diffusion tensor imaging of P4 rat pups acquired 24 h after exposure to lipopolysaccharide (LPS). (a) Coronal DTI images of LPS exposed animal (top row) and 0.9% NaCl exposed animal (bottom row). RGB (red, green, and blue) map in which colors represent the preferred direction of water diffusion. Red corresponds to medial–lateral, green to superior–inferior, and blue to rostral–caudal directions. The region of interest over the corpus callosum is highlighted in yellow. Note the restricted diffusion in the apparent diffusion coefficient (ADC) map of a pup exposed to LPS (arrow). (b) Bar graph of the diffusivity in the corpus callosum. Note the significant decrease in ADC and axial and radial diffusivity in animals exposed to LPS. (c) Bar graph of the diffusivity in the striatum. Note the significant decrease in ADC as well as radial diffusivity in animals exposed to LPS (* $P < 0.0001$, ** $P < 0.0005$, † $P < 0.05$).

amoeboid cells localized on the edge of the corpus callosum with a cluster in the cingulum. Quantification of microglial activation 24 h after LPS exposure by immunohistochemistry revealed a strong bilateral reaction along the corpus callosum, especially in the cingulum. Both surface area covered by CD68 expression (LPS: 5315 ± 548 , NaCl: 720 ± 151 μm^2 ; $P = 0.0001$) and cell count (LPS: 211 ± 10 , NaCl: 57 ± 13 ; $P = 0.0001$) within a predefined region of interest were significantly increased in animals exposed to LPS (Figure 3).

Astrogliosis. LPS exposure was further followed by an intense astroglial reaction just 24 h after exposure (Figure 4a,b) disseminated throughout the brain, especially in the cortex and the external capsule, with a very strong immunofluorescence. We found very little, if any, astroglial response in the corpus callosum. Quantification of astrogliosis revealed a very strong reaction in the cortex (LPS: 109654 ± 16279 , NaCl: 15226 ± 9349 μm^2 ; $P = 0.0002$) and in the hippocampus (LPS: 425360 ± 51878 , NaCl: 150354 ± 32966 μm^2 ; $P = 0.0007$). It also revealed a significant reaction in the cingulum (LPS: 32769 ± 7849 , NaCl: 11415 ± 3421 μm^2 ; $P = 0.02$) and a strong reaction in the external capsule (LPS: 21505 ± 3137 , NaCl: 7746 ± 1678 μm^2 ; $P = 0.001$).

Apoptosis. LPS exposure triggered significant apoptosis when evaluated by immunohistochemistry, 24 h after exposure. Caspase-3 activation was shown to be still present 24 h after injection of LPS and was predominant around the injection site, predominantly in the cortex. There was little caspase-3 activation in the corpus callosum (data not shown). Fractin immunohistochemistry, another marker of apoptosis that detects caspase-cleaved fragments of actin, revealed a very strong reaction at the site of injection, along the upper half of the corpus callosum, in the cingulum, and in the striatum (Figure 5). Fractin quantification with immunohistochemistry revealed a significant increase in the corpus callosum (LPS: 5898 ± 1455 , NaCl: 286 ± 125 μm^2 ; $P = 0.001$; Figure 5c). Due to the very nature of fractin expression and localization, we wanted to determine whether the degree of ADC reduction in the corpus callosum would identify brains with widespread fractin expression. Indeed, we found a highly significant linear regression between the ADC and the natural logarithm of fractin surface: $\ln(\text{fractin surface } \mu\text{m}^2) = -14.34 \times \text{ADC} + 22.72$; $R^2 = 0.53$; $P = 0.0002$; Figure 5d).

RNA Expression

The expressions of the cDNAs for IL-1 β , IL-6, and TNF- α in whole brain were determined by quantitative real-time PCR.

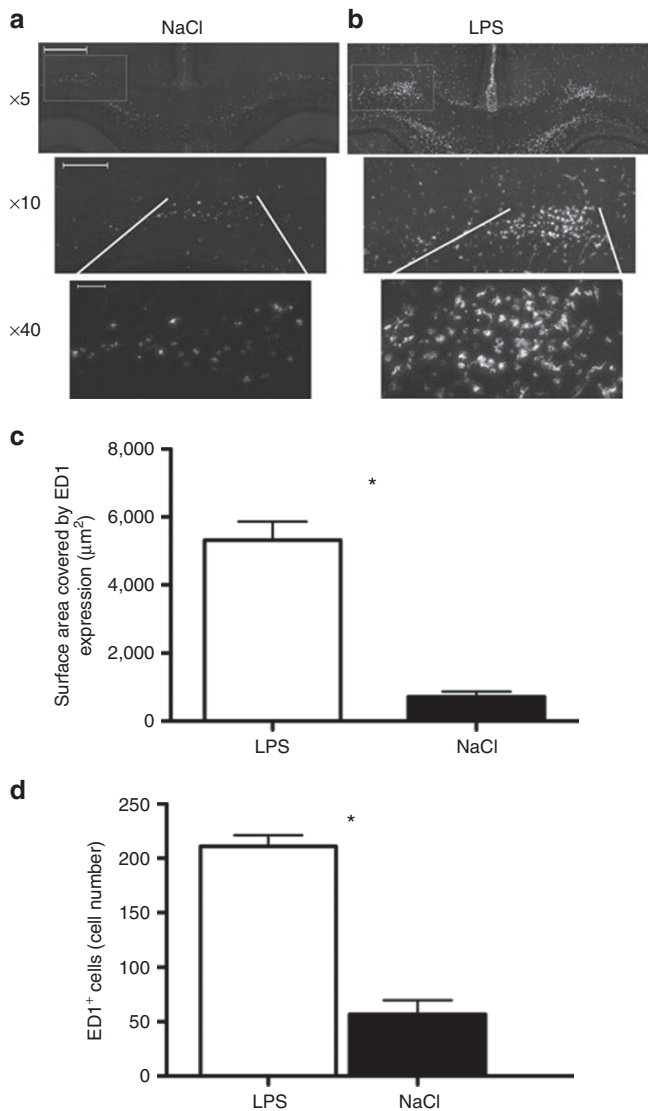


Figure 3. Immunohistochemistry of activated microglia (ED1) in animals exposed to (a) 0.9% NaCl or (b) lipopolysaccharide (LPS). Note the strong microglial reaction along the corpus callosum, with a well-defined increase in expression in the cingulum of animals exposed to LPS. (c) Bar graph of the surface area covered by ED1 expression in the cingulum. (d) Bar graph of the cell number in the cingulum. Note the significant increase in both ED1 expression and ED1-positive cell number in animals exposed to LPS (* $P < 0.0001$). Bar at 5 \times = 500 μm , 10 \times = 200 μm , and 40 \times = 50 μm .

The analysis revealed a very strong inflammatory response in P4 rat pups 24 h after LPS exposure, with an increase in all three cytokines tested (Figure 6).

DISCUSSION

We characterized, by high-field MRI and proton MRS (¹H-MRS), the acute inflammatory white matter injury in very immature rat pups corresponding to 24–28 wk of human gestation. Extensive immunohistochemical evaluation and quantification of inflammatory markers were studied in detail to understand the underlying tissue changes seen in brain MRI. The use of the spin echo full-intensity acquired localized pulse sequence (SPECIAL) enabled us to get a high-resolution

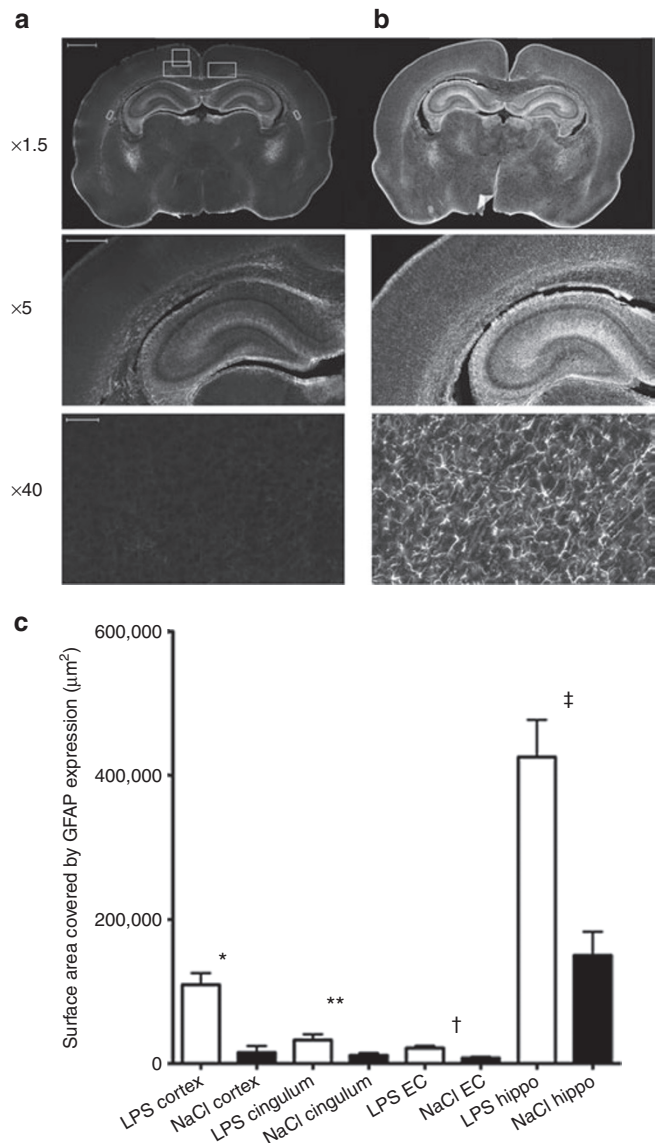


Figure 4. Immunohistochemistry with glial fibrillary acidic protein (GFAP) for astrogliosis in animals exposed to (a) 0.9% NaCl or (b) lipopolysaccharide (LPS). Note the massive astrogliosis in animals exposed to LPS. (c) Bar graph of the surface area covered by GFAP expression in the cortex, cingulum, external capsule (EC), and the hippocampus (hippo). Note the significant increase in GFAP expression in animals exposed to LPS in these four regions of interest (* $P = 0.0002$, ** $P = 0.02$, † $P = 0.001$, ‡ $P = 0.0007$). Bar at 1.5 \times = 1,000 μm , 5 \times = 500 μm , and 40 \times = 50 μm . In the top row of panel a, boxed areas represent the placement of regions of interest.

spectrum in a limited amount of time from a very small voxel (25). The very short echo time also allowed us to quantify macromolecule peaks normally not visible at longer echo time. Quantification using the LCModel showed a significant increase in lactate and identified free lipids, with a marginal increase in macromolecules in animals exposed to LPS (Figure 1). Yet, the quantification of macromolecules should be interpreted with caution, because this is not a single individual peak but an underlying broad spectrum. Similar to our findings, there are several pathological processes affecting the white matter such as multiple sclerosis, adrenoleukodystrophy,

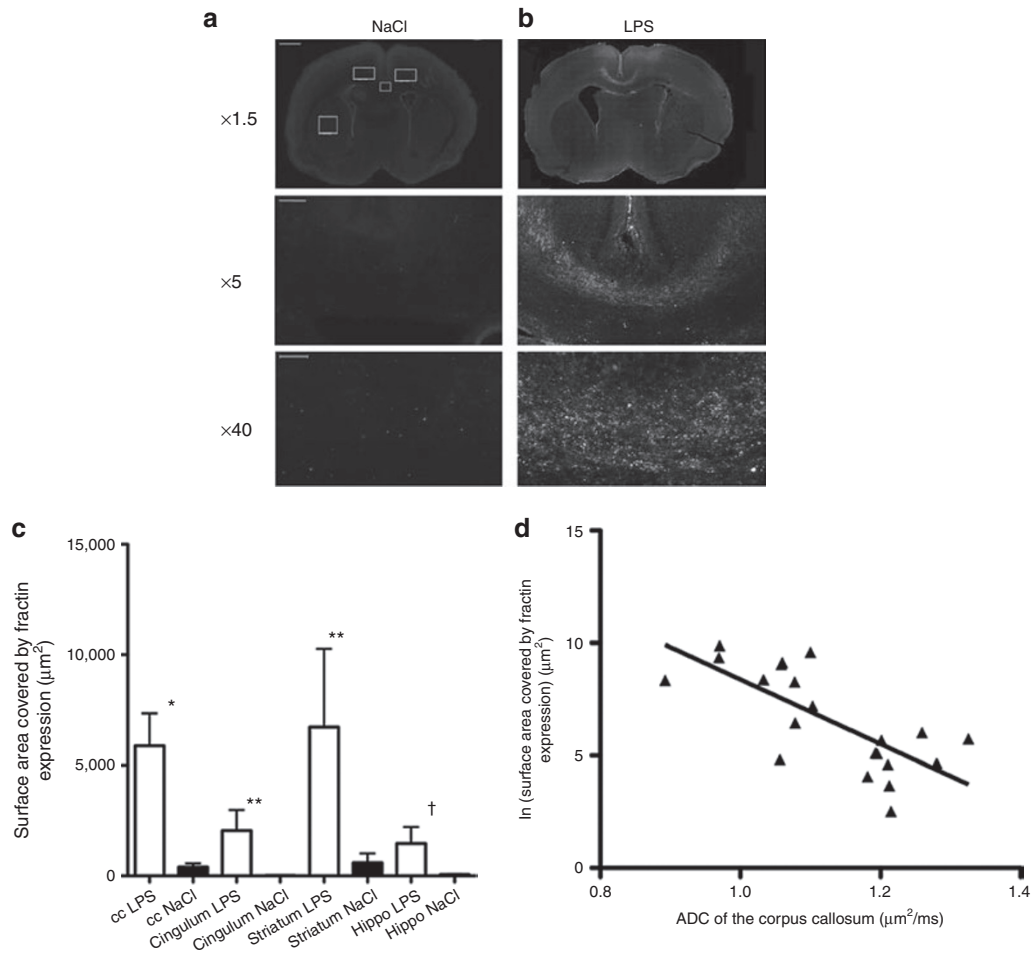


Figure 5. Immunohistochemistry with fractin for apoptosis in animals exposed to 0.9% NaCl (**a**) or lipopolysaccharide (LPS) (**b**). Note the increase of fractin in animals exposed to LPS. (**c**) Bar graph of the surface area covered by fractin expression in the corpus callosum (cc), cingulum, striatum, and hippocampus (Hippo). Note the significant increase in fractin expression in animals exposed to LPS in these four regions of interest (* $P < 0.001$, ** $P < 0.005$, † $P < 0.01$). (**d**) Scatter plot of the apparent diffusion coefficient (ADC) effect for the natural logarithm of the fractin quantification in the corpus callosum, with the following regression line: $\ln(\text{fractin}) = -14.34 \times \text{ADC} + 22.72$; $R^2 = 0.53$, $P = 0.0002$. Bar at $1.5\times = 2,000 \mu\text{m}$, $1\times = 200 \mu\text{m}$, and $40\times = 50 \mu\text{m}$. In panel **a**, top row, boxed areas represent the placement of regions of interest.

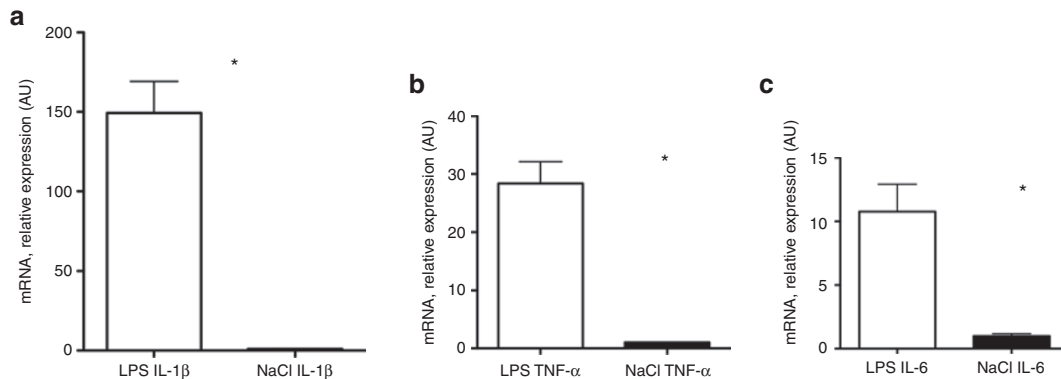


Figure 6. Effect of lipopolysaccharide on gene expression in brain in P4 rat pups 24 h after exposure. Relative mRNA levels (in arbitrary units (AU)) of (a) interleukin (IL)-1β, (b) TNF-α, and (c) IL-6 in the brain (* $P < 0.05$).

and stroke, which are associated with an increase in the lactate and lipid peaks (26–28). The underlying substrate for the increased lipids is a difficult topic that has been addressed in a detailed evaluation of ¹H MR spectroscopy in an animal model

of glioma, showing that the induction of apoptosis was associated with a major increase of the lipid peak at 0.9 and 1.3 ppm corresponding to the –CH₃ and –CH₂ groups respectively (29). In clinical settings, an increase in lactate and macromolecules

has also been seen in newborns after hypoxic–ischemic injury at short echo times (30). Clinical research in preterm infants at term-equivalent age showed an increase in lactate/creatine ratio in infants with white matter damage (31), with no data available on lipids due to the long echo time used. Indeed, clinical spectroscopy usually uses echo times ranging from 140 to 280 ms, in which range macromolecules are not measurable due to their short T₂, and precious quantifiable changes of macromolecules or lipids are lost. On the other hand, lactate can be quantified reliably even at long echo times. In our study, the increase in lactate was seen predominantly in males corresponding to epidemiological (32) and laboratory studies showing an increased vulnerability of the preterm male brain independent of hormonal exposure, with gender-related differences in the apoptotic pathway found in animal models of immature brain injury and, interestingly, even a differential response to neuroprotection (33–35).

Recent animal studies, using a hypoxic–ischemic model, have found that the degree of ADC restriction could not only detect injury but also serve as a noninvasive method to quantify apoptosis (36). Moreover, the induction of apoptosis in a macrophage cell line by LPS and interferon- γ exposure resulted in ADC reduction (37). In our study, we characterized acute white matter inflammatory injury in a very immature brain as a significant reduction of ADC along the corpus callosum associated with a decrease in radial and axial diffusivity (Figure 2). A study performing a Monte Carlo simulation, confirmed by an MR experiment in the adult sciatic nerve, has shown that beading of the neurite membrane introduces barriers along the main axis, limiting water mobility along this axis, thus causing a reduction of axial diffusivity as well as an increased tortuosity that affects both axial and radial diffusivity (38). In the brain, neuritic beading, seen in epilepsy, trauma, ischemia, aging, and neurodegenerative diseases, was shown to lead to neuronal cell death (39). When transposing this concept to the immature brain, the fractin expression found in our study may reflect underlying axonal injury that could explain the reduction of axial and radial diffusivity. The degree of ADC reduction in the white matter at 24 h is more profound than that in our previous study, wherein the first MRI was performed on the same day following LPS injection (21). Indeed, it appears that by combining knowledge about ADC evolution after injury in hypoxic–ischemic insults with our experiments on LPS exposure, the nadir of ADC reduction seems to be 24 h after insult. The acute DTI changes secondary to inflammation were also evaluated in the striatum, depicting a significant reduction of ADC and radial diffusivity, which was less profound than that in the corpus callosum and not as readily identifiable on images. Still, as discussed later, striatal injury has been shown in the very preterm population (40).

The corpus callosum in the days following LPS exposure was shown to have a decreased cell density (21). Looking more specifically at cell types that could have an effect on MR findings, we looked at microglial activation and astrogliosis. There was diffuse astrogliosis, similar to what has been described in PVL affecting humans (8). As in mice pups (36), 24 h were sufficient

to produce a massive astroglial response in rat pups. There was a strong astroglial response in the external capsule, in the cortex, and in the cingulum adjacent to the pathway of the corpus callosum, but no signs of astrogliosis at the central part of the corpus callosum (Figure 4), in accordance with the absence of astrogliosis in this area described 96 h post-LPS exposure (21). To date, there is no clear explanation for the phenomenon. There was very strong microglial activation, with wide amoeboid microglial cell bodies along the corpus callosum with a cluster at the level of the cingulum, seen only in rats exposed to LPS (Figure 3), similarly to what has been described in humans (8)—but barely any microglial cell at the center of the corpus callosum. LPS exposure in P3 Wistar rats produced significant increase of IL-1, IL-6, and TNF- α by real-time PCR, confirming the active inflammatory status in line with what has been previously published in P5 Sprague–Dawley rats (20,23). To correlate changes seen on DTI and immunohistochemical evaluation, and in light of well-described axonal damage seen in human newborn brains with PVL (9), we looked at a marker of caspase-cleaved actin, namely fractin, in the corpus callosum. Interestingly, fractin was readily identified in the corpus callosum and in the cingulum in animals exposed to LPS (Figure 5). The study was able to reproduce in an animal model evidence of axonal disruption seen in human preterm infants with PVL. Interestingly, we found a strong increase in fractin expression in the striatum, similarly to prenatal exposure to LPS causing an increase in apoptotic cell death measured by TUNEL (terminal deoxynucleotidyl transferase nick end labeling) (41). Indeed, the inflammatory brain injury of the preterm infant is a global process, with evidence in older children born preterm of a diffuse vulnerability that includes the striatum (42). Among the group exposed to LPS, it appeared that some animals had a more diffuse and intense fractin immunohistological fluorescence and indeed, we found a significant linear regression between the degree of ADC reduction and the natural logarithm of the surface area covered by fractin, suggesting that the ADC can be used as a marker of neuroaxonal damage quantification in these settings. These findings can explain, in part, how ADC reduction in the posterior limb of the internal capsule was shown to correlate with poor outcome in asphyxiated human newborns in a clinical study (43), wherein a significant restriction of diffusion of the white matter highlights massive axonal degeneration.

Conclusion

Using this new approach of injecting LPS under ultrasound guidance into the very immature rat brain, we were able to have a minimally invasive procedure that revealed to be extremely robust, with a spectroscopic signature and diffusion changes matching closely those seen in clinical settings. Quantification of the changes induced by inflammation was possible both by ¹H-MRS and DTI. High-field ¹H-MRS was able to quantify an increase in lactate in the white matter of 4-d-old rat pups in a voxel volume of less than 8 μ l. The very clear visualization of the profound ADC reduction primarily in the white matter in the setting of an inflammatory injury, together with a

strong correlation with signs of axonal damage quantified on immunohistochemistry, suggests high-field MRI as a potential noninvasive biomarker of inflammatory white matter injury in the developing brain.

METHODS

Animal Preparation

Animal-handling procedures were approved by the Office Vétérinaire Cantonal (Geneva) in accordance with Swiss federal laws. P3 Wistar rats, anesthetized with isoflurane, were injected under ultrasound guidance with LPS (1 mg/kg) suspension (*Escherichia coli*, serotype 055:B5; Sigma, St Louis, MO) in 0.5 µl of sterile saline or with the same volume of sterile saline alone for the sham group. The injection was placed in the corpus callosum at the level equivalent to P-7, c9 (44). Injections were made with a micropipette mounted on a microprocessor-controlled injector (Nanoliter 2000; World Precision Instruments, Aston, Stevenage, UK; see **Supplementary Figure S1** online). The injections themselves could be visualized by ultrasonography, thus increasing the efficiency of the intervention when comparing with stereotaxic injection with up to 1/3 of misplaced injections (21). Twenty-two pups were injected with LPS, 2 of which died; 15 pups were injected with saline alone.

Nuclear Magnetic Resonance

All ¹H MRS/DTI studies were acquired on an actively shielded 9.4-T/31-cm bore magnet (Magnex Scientific, Abingdon, UK) with a 12-cm gradient set (400 mT/m in 120 µs) connected to a DirectDrive console (Varian Associates, Palo Alto, CA). Ten pups were not scanned due to time constraint (6 LPS, 4 NaCl). For the MRI acquisition, animals were anesthetized with isoflurane (0.5–2%). Spectroscopy acquisitions were performed in a custom-built ertalyte MRI-compatible head holder with a homebuilt quadrature surface coil consisting of two geometrically decoupled 14-mm-diameter single loops. An actively decoupled Alderman coil was used with the quadrature coil as a transmit coil for imaging. Body temperature was monitored and maintained stable at 36 °C. Respiration rate was monitored using a custom-built pressure pillow placed under the rat's abdomen. A fast spin echo MRI sequence (repetition time = 3,500 ms, echo train length = 8, echo spacing = 13 ms, effective echo time = 78 ms) was used to obtain anatomical images with an in-plane resolution of 58 × 117 µm² and a slice thickness of 600 µm. Based on these images, a volume of interest (1 × 3 × 2.5 mm³) for spectroscopy was centered on the corpus callosum (**Figure 1a**). Magnetic field homogeneity was adjusted using FASTMAP (45). (Mean line width of water resonance was 14.3 ± 2.4 Hz.) Localized ¹H MRS was obtained with the very short echo time (2.8 ms) SPECIAL sequence (25). This sequence is based on a combination of the one-dimensional image-selected *in vivo* spectroscopy technique and a slice-selective spin echo sequence. The sequence was preceded by an efficient water signal suppression and outer volume saturation module. The water suppression, which was interleaved with outer volume saturation, was accomplished by a series of seven 25-ms variable power radio frequency pulses with optimized relaxation delays. To further improve the efficiency of water suppression, another frequency-selective saturation pulse (15 ms Gaussian; bandwidth = 180 Hz) was added in the delay between the adiabatic slice-selective inversion pulse and the spin echo module. All spectra were acquired with a spectral width of 5 kHz, 4,095 complex data

points, and a repetition time of 4 s. Water spectrum was acquired as a reference for quantification, and then the metabolite spectrum was acquired using water suppression. Spectra were acquired in 15 blocks of 16 averages stored separately on disk for a total acquisition time of 16 min. Metabolite concentrations were quantified/estimated using the LCMoDel. A Cramér–Rao lower bound with a threshold set below 20% identified quantifiable metabolites. Coronal diffusion-weighted images were acquired with a spin echo sequence with repetition time = 2 s, echo time (TE) = 36 ms, 2 averages, slice thickness = 600 µm, nominal in-plane resolution (pixel size) at P4 = 117 × 234 µm. Images were then interpolated in the phase-encoding direction, resulting in a final resolution of 117 × 117 µm. The delay between application of the diffusion gradient pulses (Δ) was set to 21 ms, the application time (δ) was set to 7 ms, with b value amplitudes = 0 and 840 s/mm². Two sets of six directions were applied in an origin-symmetric fashion to minimize the background magnetic field gradient effect in the diffusion measurement. Color-coded (red, green, and blue (RGB)) ADC and axial and radial diffusivity maps were generated, allowing the placement of a region of interest over the corpus callosum, the striatum, and a reference region below the corpus callosum (see **Supplementary Figure S2** online) and the quantification of the ADC axial and radial diffusivity on the same region of interest as previously described (**Figure 2**) (21).

Histology

After MR imaging, the rats received a lethal injection of ketamine and lidocaine and were transcardially perfused with saline, which was followed by 4% paraformaldehyde. Brains were extracted and immersion-fixed in 4% paraformaldehyde for 24 h at 4 °C and then cryoprotected by immersion in 30% sucrose for at least 24 h. Coronal sections (50 µm thick) were cut on a cryostat and conserved at –20°C in a cryoprotectant solution (30% ethylene glycol, 0.03 mol/l PO₄ (phosphate-buffered saline), 15% sucrose) until staining. Special care was taken to ensure that the midline of the brain was absolutely perpendicular to the blade for cutting coronal sections. Similarly, when MRI sections were obtained, the animals were carefully positioned by placing them in a custom-built MRI-compatible neonatal head holder in ertalyte. This allowed for high degree of correspondence between MRI and histology. Immunohistochemistry was performed on five brain sections 300 µm apart for each animal using the polyclonal rabbit antibodies anti-glial fibrillary acidic protein ((GFAP) 1:400; DakoCytomation, Glostrup, Denmark) to detect astrogliosis, anti-fractin (1:500; Millipore, Billerica, MA)—a marker of apoptosis that detects caspase-cleaved fragments of actin—and mouse monoclonal antibodies CD68 (1:500; Abcam, Cambridge, UK) to detect microglial activation. Sections were washed in phosphate-buffered saline three times. Nonspecific binding was blocked with 1% bovine serum albumin, 3% normal goat serum (Sigma-Aldrich, Buchs, Switzerland), and 0.3% Triton X-100 (Sigma-Aldrich). Primary antibodies were applied to free-floating sections overnight at 4 °C with 1% bovine serum albumin, 1% normal goat serum (Sigma-Aldrich), and 0.3% Triton X-100 (Sigma-Aldrich). Sections were then washed and incubated first with 4',6-diamidino-2-phenylindole, followed by species-specific secondary fluorescent antibodies: Alexa fluor 555 goat anti-mouse immunoglobulin G (1:1,000; Invitrogen, Basel, Switzerland) and Alexa fluor 488 goat anti-rabbit immunoglobulin G (1:1,000; Invitrogen).

Slides were digitized at 20× with the Mirax Midi (Carl Zeiss MicroImaging GmbH, Jena, Germany). Quantification of pixels above a defined threshold identical in both groups (to remove

Table 1. List of primers

	Forward	Reverse
IL-1	5'-GGCAACTGCCCTGAACTCAA-3'	5'-GCCTCAAAGAACAGGTCATTCTC-3'
IL-6	5'-ATATGTTCTCAGGGAGATCTTGGA-3'	5'-TGCATCATCGCTGTTTCATACAA-3'
TNF-α	5'-GACCCTCACACTCAGATCATCTTCT-3'	5'-TCCGCTTGTTGGTTTGCTA-3'
RPS29	5'-GCCAGGGTTCGCTCTTG-3'	5'-GGCACATGTTACGCCGAT-3'

IL, interleukin; RPS, ribosomal protein; TNF, tumor necrosis factor.

background) was performed with the software Mercator (Explora Nova, La Rochelle, France) in a rectangular region of interest with fixed dimensions (Figures 3–5) on five brain sections 300 μm apart, allowing the quantification of pixels covered by immunofluorescent cells and their processes (21). The quantification of GFAP was localized in the left and right external capsule, the cortex, the hippocampus, and the left and right cingulum. The quantification of fractin was localized in the corpus callosum and in the left and right cingulum. The quantification of microglial activation was localized in the left and right cingulum. The quantification of microglial reaction also included an automatic quantification of cell count in the cingulum.

RNA Preparation and Gene Expression Analysis

Total RNA from brain was extracted from four pups exposed to LPS and four pups exposed to NaCl, using the RNeasy Mini Kit according to the manufacturer's protocol (Qiagen, Basel, Switzerland). Total RNA (2 μg) was reverse-transcribed using 400 units of Moloney Murine Leukemia Virus Reverse Transcriptase (Invitrogen), in the presence of 1 unit/ μl RNasin (Promega, Madison, WI), 0.2 μg of random primers (oligo(dN)6; Promega), 2 mmol/l dNTPs (deoxynucleotide triphosphates), and 20 $\mu\text{mol/l}$ of dithiothreitol (Invitrogen). The expression of the cDNAs for rat IL-1, IL-6, and TNF- α in whole brain was determined by quantitative real-time PCR using an ABI StepOne Plus Sequence Detection System (Applied Biosystems, Rotkreuz, Switzerland) and was normalized using the housekeeping ribosomal gene RPS29. PCR products were quantified using the Master SYBR Green mix (Applied Biosystems), and results are expressed in arbitrary units (AU). Primers were designed using the Primer Express software (Applied Biosystems), chosen when possible on both sides of an intron to avoid amplification of eventual contaminating genomic DNA. Oligos were used at 217 nmol/l each (Microsynth, Balgach, Switzerland). The sequence of the primers used is provided in Table 1.

Statistics

All data are presented as mean \pm SEM. Comparisons between groups were performed using a Student's *t*-test if the data were distributed normally; otherwise, a Mann-Whitney test was used. Statistical significance was set below 0.05. Analyses were performed using GraphPad Prism (GraphPad Software, La Jolla, CA).

SUPPLEMENTARY MATERIAL

Supplementary material is linked to the online version of the paper at <http://www.nature.com/pr>

STATEMENT OF FINANCIAL SUPPORT

This study was supported by the Swiss National Fund 33CM30-124101, the Centre d'Imagerie BioMédicale of the University of Lausanne, University of Geneva, University Hospital of Geneva, Centre Hospitalier Universitaire Vaudois, École Polytechnique de Lausanne, and the Boninchi, De Reuter, Leenaards and Jeantet Foundations in Switzerland.

REFERENCES

- Volpe JJ. Brain injury in premature infants: a complex amalgam of destructive and developmental disturbances. *Lancet Neurol* 2009;8:110–24.
- Fazzi E, Bova S, Giovenzana A, Signorini S, Uggetti C, Bianchi P. Cognitive visual dysfunctions in preterm children with periventricular leukomalacia. *Dev Med Child Neurol* 2009;51:974–81.
- Anderson PJ, De Luca CR, Hutchinson E, Spencer-Smith MM, Roberts G, Doyle LW; Victorian Infant Collaborative Study Group. Attention problems in a representative sample of extremely preterm/extremely low birth weight children. *Dev Neuropsychol* 2011;36:57–73.
- Inder TE, Anderson NJ, Spencer C, Wells S, Volpe JJ. White matter injury in the premature infant: a comparison between serial cranial sonographic and MR findings at term. *AJNR Am J Neuroradiol* 2003;24:805–9.
- Maalouf EF, Duggan PJ, Counsell SJ, et al. Comparison of findings on cranial ultrasound and magnetic resonance imaging in preterm infants. *Pediatrics* 2001;107:719–27.
- Hagmann CF, De Vita E, Bainbridge A, et al. T2 at MR imaging is an objective quantitative measure of cerebral white matter signal intensity abnormality in preterm infants at term-equivalent age. *Radiology* 2009;252:209–17.
- Woodward LJ, Anderson PJ, Austin NC, Howard K, Inder TE. Neonatal MRI to predict neurodevelopmental outcomes in preterm infants. *N Engl J Med* 2006;355:685–94.
- Banker BQ, Larroche JC. Periventricular leukomalacia of infancy. A form of neonatal anoxic encephalopathy. *Arch Neurol* 1962;7:386–410.
- Haynes RL, Billiards SS, Borenstein NS, Volpe JJ, Kinney HC. Diffuse axonal injury in periventricular leukomalacia as determined by apoptotic marker fractin. *Pediatr Res* 2008;63:656–61.
- Inder TE, Warfield SK, Wang H, Hüppi PS, Volpe JJ. Abnormal cerebral structure is present at term in premature infants. *Pediatrics* 2005;115:286–94.
- Inder TE, Hüppi PS, Warfield S, et al. Periventricular white matter injury in the premature infant is followed by reduced cerebral cortical gray matter volume at term. *Ann Neurol* 1999;46:755–60.
- Dammann O, Kuban KC, Leviton A. Perinatal infection, fetal inflammatory response, white matter damage, and cognitive limitations in children born preterm. *Ment Retard Dev Disabil Res Rev* 2002;8:46–50.
- Sizonenko SV, Sirimanne E, Mayall Y, Gluckman PD, Inder T, Williams C. Selective cortical alteration after hypoxic-ischemic injury in the very immature rat brain. *Pediatr Res* 2003;54:263–9.
- Debillon T, Gras-Leguen C, Leroy S, Caillon J, Rozé JC, Gressens P. Patterns of cerebral inflammatory response in a rabbit model of intrauterine infection-mediated brain lesion. *Brain Res Dev Brain Res* 2003;145:39–48.
- Dean JM, van de Looij Y, Sizonenko SV, et al. Delayed cortical impairment following lipopolysaccharide exposure in preterm fetal sheep. *Ann Neurol* 2011;70:846–56.
- Eklind S, Mallard C, Leverin AL, et al. Bacterial endotoxin sensitizes the immature brain to hypoxic-ischaemic injury. *Eur J Neurosci* 2001;13:1101–6.
- van de Looij Y, Lodygensky GA, Dean J, et al. High-field diffusion tensor imaging characterization of cerebral white matter injury in lipopolysaccharide-exposed fetal sheep. *Pediatr Res* 2012;72:285–92.
- Favrais G, van de Looij Y, Fleiss B, et al. Systemic inflammation disrupts the developmental program of white matter. *Ann Neurol* 2011;70:550–65.
- Brehmer F, Bendix I, Prager S, et al. Interaction of inflammation and hyperoxia in a rat model of neonatal white matter damage. *PLoS ONE* 2012;7:e49023.
- Cai Z, Pang Y, Lin S, Rhodes PG. Differential roles of tumor necrosis factor- α and interleukin-1 beta in lipopolysaccharide-induced brain injury in the neonatal rat. *Brain Res* 2003;975:37–47.
- Lodygensky GA, West T, Stump M, Holtzman DM, Inder TE, Neil JJ. *In vivo* MRI analysis of an inflammatory injury in the developing brain. *Brain Behav Immun* 2010;24:759–67.
- Fan LW, Tien LT, Mitchell HJ, Rhodes PG, Cai Z. Alpha-phenyl-n-tert-butyl-nitron ameliorates hippocampal injury and improves learning and memory in juvenile rats following neonatal exposure to lipopolysaccharide. *Eur J Neurosci* 2008;27:1475–84.
- Pang Y, Cai Z, Rhodes PG. Disturbance of oligodendrocyte development, hypomyelination and white matter injury in the neonatal rat brain after intracerebral injection of lipopolysaccharide. *Brain Res Dev Brain Res* 2003;140:205–14.
- Clancy B, Darlington RB, Finlay BL. Translating developmental time across mammalian species. *Neuroscience* 2001;105:7–17.
- Mlynárik V, Gambarota G, Frenkel H, Gruetter R. Localized short-echo-time proton MR spectroscopy with full signal-intensity acquisition. *Magn Reson Med* 2006;56:965–70.
- Cianfoni A, Niku S, Imbesi SG. Metabolite findings in tumefactive demyelinating lesions utilizing short echo time proton magnetic resonance spectroscopy. *AJNR Am J Neuroradiol* 2007;28:272–7.
- Oz G, Tkáč I, Charnas LR, et al. Assessment of adrenoleukodystrophy lesions by high field MRS in non-sedated pediatric patients. *Neurology* 2005;64:434–41.
- Saunders DE, Howe FA, van den Boogaart A, Griffiths JR, Brown MM. Discrimination of metabolite from lipid and macromolecule resonances

- in cerebral infarction in humans using short echo proton spectroscopy. *J Magn Reson Imaging* 1997;7:1116–21.
29. Hakumäki JM, Poptani H, Sandmair AM, Ylä-Herttuala S, Kauppinen RA. ¹H MRS detects polyunsaturated fatty acid accumulation during gene therapy of glioma: implications for the *in vivo* detection of apoptosis. *Nat Med* 1999;5:1323–7.
 30. Cecil KM, Jones BV. Magnetic resonance spectroscopy of the pediatric brain. *Top Magn Reson Imaging* 2001;12:435–52.
 31. Robertson NJ, Kuint J, Counsell TJ, et al. Characterization of cerebral white matter damage in preterm infants using ¹H and ³¹P magnetic resonance spectroscopy. *J Cereb Blood Flow Metab* 2000;20:1446–56.
 32. Hintz SR, Kendrick DE, Vohr BR, Kenneth Poole W, Higgins RD; Nichd Neonatal Research Network. Gender differences in neurodevelopmental outcomes among extremely preterm, extremely-low-birthweight infants. *Acta Paediatr* 2006;95:1239–48.
 33. Johnston MV, Hagberg H. Sex and the pathogenesis of cerebral palsy. *Dev Med Child Neurol* 2007;49:74–8.
 34. Renolleau S, Fau S, Charriaut-Marlangue C. Gender-related differences in apoptotic pathways after neonatal cerebral ischemia. *Neuroscientist* 2008;14:46–52.
 35. Nijboer CH, Kavelaars A, van Bel F, Heijnen CJ, Groenendaal F. Gender-dependent pathways of hypoxia-ischemia-induced cell death and neuroprotection in the immature P3 rat. *Dev Neurosci* 2007;29:385–92.
 36. Lodygensky GA, West T, Moravec MD, et al. Diffusion characteristics associated with neuronal injury and glial activation following hypoxia-ischemia in the immature brain. *Magn Reson Med* 2011;66:839–45.
 37. Hortelano S, García-Martín ML, Cerdán S, Castrillo A, Alvarez AM, Boscá L. Intracellular water motion decreases in apoptotic macrophages after caspase activation. *Cell Death Differ* 2001;8:1022–8.
 38. Budde MD, Frank JA. Neurite beading is sufficient to decrease the apparent diffusion coefficient after ischemic stroke. *Proc Natl Acad Sci USA* 2010;107:14472–7.
 39. Takeuchi H, Mizuno T, Zhang G, et al. Neuritic beading induced by activated microglia is an early feature of neuronal dysfunction toward neuronal death by inhibition of mitochondrial respiration and axonal transport. *J Biol Chem* 2005;280:10444–54.
 40. Pierson CR, Folkert RD, Billiards SS, et al. Gray matter injury associated with periventricular leukomalacia in the premature infant. *Acta Neuropathol* 2007;114:619–31.
 41. Rousset CI, Chalon S, Cantagrel S, et al. Maternal exposure to LPS induces hypomyelination in the internal capsule and programmed cell death in the deep gray matter in newborn rats. *Pediatr Res* 2006;59:428–33.
 42. Nosarti C, Giouroukou E, Healy E, et al. Grey and white matter distribution in very preterm adolescents mediates neurodevelopmental outcome. *Brain* 2008;131(Pt 1):205–17.
 43. Hunt RW, Neil JJ, Coleman LT, Kean MJ, Inder TE. Apparent diffusion coefficient in the posterior limb of the internal capsule predicts outcome after perinatal asphyxia. *Pediatrics* 2004;114:999–1003.
 44. Ramachandra R, Subramanian T. *Atlas of the Neonatal Rat Brain*, 1st edn. CRC Press, Boca Raton, FL, 2011.
 45. Gruetter R. Automatic, localized *in vivo* adjustment of all first- and second-order shim coils. *Magn Reson Med* 1993;29:804–11.